

Intervalley interactions in Si quantum dots

Doyeol Ahn^{a)}

Department of Electrical and Computer Engineering and Institute of Quantum Information Processing and Systems, University of Seoul, Seoul 130-743, Republic of Korea

(Received 21 October 2004; accepted 14 June 2005; published online 8 August 2005)

In this paper, we studied the intervalley interactions between the orbital functions associated with multivalley of silicon (Si) quantum dots. Numerical calculations show that the intervalley coupling between orbital functions increases rapidly with an applied electric field. We also considered the potential applications to quantum bit operation utilizing controlled intervalley interactions. Quantum bits are the multivalley symmetric and antisymmetric orbitals. Evolution of these orbitals would be controlled by an external electric field which turns on and off the intervalley interactions. Estimates of the decoherence time are made for the longitudinal-acoustic-phonon process. Elementary single- and two-qubit gates are also proposed. © 2005 American Institute of Physics.

[DOI: 10.1063/1.1994946]

I. INTRODUCTION

It is well known that the lowest conduction band of an ideal Si crystal has six equivalent minima of ellipsoidal shape along the [100] direction as shown in Fig. 1. These ellipsoids are often called valleys and the total wave function of the ground state is obtained from a linear combination of the six wave functions, each localized around one of the Δ_1 conduction-band minima. The overlap of wave functions associated with different valleys is assumed to be negligible. In the study of early quantum structures such as n -channel inversion layer on the Si (001) surface, it was found that the broken translation symmetry lifts the sixfold degeneracy into the twofold degenerate valleys located near the X point in the $\langle 001 \rangle$ direction in the k space and the fourfold degenerate valleys in the direction normal to the surface.¹

In addition, there were experimental observations²⁻⁴ of anomalous structures in the gate-voltage dependence of the conductivity of vicinal planes of Si (100) n -channel inversion layers. It has been suggested that these anomalous structures are caused by the lifting of the twofold valley degeneracy in the $\langle 001 \rangle$ direction as a result of the valley-valley interaction.^{5,6} The splitting is proportional to the gradient of the confinement potential normal to the surface.⁷

It would be interesting to ask whether the intervalley coupling is controllable. If this is possible, it will permit us extra degrees of freedom in silicon technology. It can also lead to potential applications to silicon-based quantum information processing. So far, most of the existing proposals for the solid-state quantum bits (qubits) are based on the electron spin confined to quantum dots,^{8,9} coherent quantum state in a Cooper-pair box,¹⁰ or the nuclear spins of impurity atoms implanted on the surface of Si.^{11,12} For the latter it still remains an experimental challenge to fabricate a structure in which each nuclei can be effectively manipulated. Recently, there have been observations of coherent oscillation of a charge qubit in a III-V double-quantum-dot¹³ and stacked coupled-quantum-dot structures.¹⁴ These results suggest that

the controlled evolution of superposed charge states in the semiconductor quantum dots would be possible. In order to implement the solid-state quantum computation, however, it is required to minimize the decoherence effects on the coherent quantum states or qubits.¹⁵ This is actually one of the requirements that must be met to make such devices good candidates for the building block of quantum computer.^{16,17} These conditions include (1) a scalable physical system with well defined qubits, (2) the ability to initialize the state of the qubits, (3) a long relevant decoherence time, much longer than the gate operation time, (4) a “universal” set of quantum gates, and (5) a qubit-specific measurement capability.

Potential drawbacks of the compound semiconductor charge qubit is the relatively short decoherence time and difficulties in fabricating double dots. There would be several merits of a silicon implementation of quantum bits. First of all, the crystal growth and processing technology for Si is quite mature. Secondly, some of the scattering processes which contribute to the decoherence such as intravalley optical-phonon processes are forbidden inherently from the group-theoretical considerations in the case of silicon. Espe-

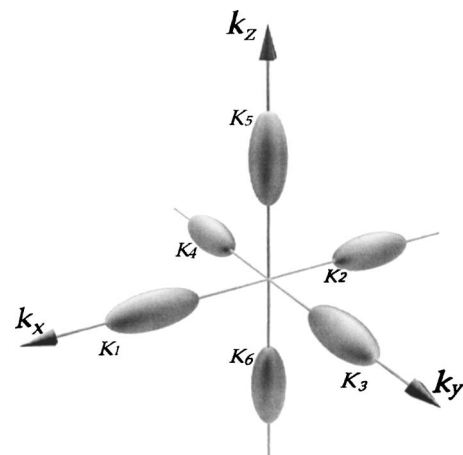


FIG. 1. The lowest conduction band of an ideal Si crystal with six equivalent minima of ellipsoidal shape along the [100] direction. For example, $K_5 = [0, 0, 0.85(2\pi/a)]$.

^{a)}Electronic mail: dahn@uos.ac.kr

cially, only the acoustic-phonon and the impurity scatterings are allowed within each ellipsoid for the intravalley processes.¹⁸ In silicon quantum dots, the situation would be more complicated than the inversion layer. The degeneracy of six valleys would be lifted into lower doublet and higher quartet in each quantization axis because of the differences of the effective masses along each axis.

In this paper, we study the intervalley interactions between the orbital functions associated with multivalley of silicon (Si) quantum dots. We also consider its potential applications to the quantum bit operation utilizing controlled intervalley interactions.

II. THEORETICAL MODEL

Let us consider a quantum dot of cubic geometry with the z direction assumed to be along the Si (001) surface. Based on the Kohn-Luttinger effective-mass theory,¹⁹ the envelope function for the quantum state in a Si quantum dot is given by

$$F(\mathbf{r}) = \sum_{\mathbf{k}} F(\mathbf{k}) \exp(i\mathbf{k} \cdot \mathbf{r}), \quad (1)$$

and

$$F(\mathbf{k}) = \sum_i \alpha_i F_i(\mathbf{k}), \quad (2)$$

where $F_i(\mathbf{k})$ is centered about the i th minimum. The constant α_i can be determined from the group-theoretical considerations.^{20–22} The equation of motion for $F_i(\mathbf{k})$ becomes^{23,24}

$$\varepsilon_i(\mathbf{k}) F_i(\mathbf{k}) + \sum_j \sum_{\mathbf{k}'} D_{\mathbf{k},\mathbf{k}'}^{ij} V(\mathbf{k} - \mathbf{k}') F_j(\mathbf{k}') = \varepsilon F_i(\mathbf{k}), \quad (3)$$

where $\varepsilon_i(\mathbf{k})$ is the energy dispersion relation of the i th valley, $V(\mathbf{k})$ is the Fourier component of the total potential, and $D_{\mathbf{k},\mathbf{k}'}^{ij}$ is the intervalley coupling term which can be derived from the cell periodic function for the conduction band as

$$\begin{aligned} D_{\mathbf{k},\mathbf{k}'}^{ij} &= D_{\mathbf{K}_i + \boldsymbol{\kappa}, \mathbf{K}_j + \boldsymbol{\kappa}'}^{ij} \\ &\cong D_{\mathbf{K}_i, \mathbf{K}_j}^{ij} + \boldsymbol{\kappa} \cdot \frac{\partial}{\partial \mathbf{K}_i} D_{\mathbf{K}_i, \mathbf{K}_j}^{ij} + \boldsymbol{\kappa}' \cdot \frac{\partial}{\partial \mathbf{K}_j} D_{\mathbf{K}_i, \mathbf{K}_j}^{ij} \\ &= I_{ij} + \boldsymbol{\kappa} \cdot \mathbf{J}_{ij} + \boldsymbol{\kappa}' \cdot \mathbf{J}'_{ij}, \end{aligned} \quad (4)$$

where \mathbf{K}_i is the wave vector at the minimum at the i th valley. Then within the frame of multivalley effective-mass theory,^{23,24} the equation of motion for $F_l(\mathbf{r}) = \sum_{\mathbf{k}} F_l(\mathbf{k}) \exp(i\mathbf{k} \cdot \mathbf{r})$ can be written down as

$$[H_l(-i\nabla) + V(\mathbf{r}) - E] F_l(\mathbf{r}) + \sum_{l' \neq l} H_{ll'}(\mathbf{r}, -i\nabla) F_{l'}(\mathbf{r}) = 0. \quad (5)$$

Here,

$$\begin{aligned} H_l(-i\nabla) &= -\frac{\hbar^2}{2m_x} \frac{\partial^2}{\partial x^2} - \frac{\hbar^2}{2m_y} \frac{\partial^2}{\partial y^2} - \frac{\hbar^2}{2m_z} \frac{\partial^2}{\partial z^2} - \frac{ie\hbar B}{2m_x} y \frac{\partial}{\partial x} \\ &\quad - \frac{ie\hbar B}{2m_y} x \frac{\partial}{\partial y} + \frac{e^2 B^2}{8} \left(\frac{x^2}{m_y} + \frac{y^2}{m_x} \right), \end{aligned} \quad (6)$$

and

$$\begin{aligned} H_{ll'}(\mathbf{r}, -i\nabla) &= I_{ll'} \exp[-i(\mathbf{K}_l - \mathbf{K}_{l'}) \cdot \mathbf{r}] [V(\mathbf{r})] \\ &\quad - i(\mathbf{J}_{ll'} \cdot \nabla) \exp[-i(\mathbf{K}_l - \mathbf{K}_{l'}) \cdot \mathbf{r}] [V(\mathbf{r})] \\ &\quad + \exp[-i(\mathbf{K}_l - \mathbf{K}_{l'}) \cdot \mathbf{r}] [V(\mathbf{r})] (-i\mathbf{J}'_{ll'} \cdot \nabla) \end{aligned} \quad (7)$$

and

$$V(\mathbf{r}) = V_c(\mathbf{r}) + e\mathbf{F} \cdot \mathbf{r}, \quad (8)$$

where m_x , m_y , and m_z are effective masses along the x , y , and z directions in each valley, E is quantized energy, \mathbf{K}_l is the wave vector at the minimum at the l th valley, $I_{ll'}$, $\mathbf{J}_{ll'}$, and $\mathbf{J}'_{ll'}$ are intervalley coupling terms, $V_c(\mathbf{r})$ is the quantum-dot confinement potential, and \mathbf{F} is an applied electric field.

In order to calculate the intervalley coupling terms, we assume that $D_{\mathbf{K}_i, \mathbf{K}_l}^{ll'}$ can be expressed by the following simple form:²⁴

$$D_{\mathbf{K}_i, \mathbf{K}_l}^{ll'} = I_{ll'} = \alpha \mathbf{e}_l \cdot \mathbf{e}_{l'} + \beta, \quad (9)$$

where \mathbf{e}_l is the unit vector in the direction of the l th axis and α and β are constants to be determined from the band-structure parameters. For example, Cardona and Pollak²⁵ gave

$$D_{(K,0,0),(0,K,0)}^{13} = 0.3915, \quad D_{(K,0,0),(-K,0,0)}^{12} = -0.2171, \quad (10)$$

with $K=0.85(2\pi/a)$ and the lattice constant $a=0.543$ nm for Si. On the other hand, Shindo and Nara²³ gave slightly different numbers. From Eq. (9) and (10), we have

$$I_{(K_0,0,0)(0,K_0,0)} = \beta = 0.3915, \quad (11)$$

$$I_{(K_0,0,0)(-K_0,0,0)} = -\alpha + 0.3915 = -0.2171,$$

which give $\alpha=0.6086$. Then from Eqs. (4) and (9)–(11), we obtain

$$I_{ll'} = \frac{1}{2}(1 + \mathbf{e}_l \cdot \mathbf{e}_{l'}) - \frac{1}{2}(1 + \mathbf{e}_l \cdot \mathbf{e}_{l'}) \cos(2\lambda_K), \quad (12)$$

and

$$\mathbf{J}_{ll'} = \frac{\partial}{\partial \mathbf{K}_l} I_{ll'} = \mathbf{e}_l \frac{\partial}{\partial K} I_{ll'} = \mathbf{e}_l (1 - \mathbf{e}_l \cdot \mathbf{e}_{l'}) \frac{\partial \lambda_K}{\partial K} \sin(2\lambda_K), \quad (13)$$

with

$$\tan(2\lambda_K) = \frac{2TK}{\varepsilon_G}, \quad (14)$$

where $T=1.08$ a.u. and $\varepsilon_G=0.268$ Ry. Here, we have included only the bases of Γ_1^u and Γ_{15} in the representation.

The most important feature of our model is that the intervalley coupling can be turned on and off by the applied

electric field. For example, the intervalley coupling between valleys 5 and 6 (along the z axis) is approximated by²⁴

$$H_{56} = -I_{56} \exp[-i(\mathbf{K}_5 - \mathbf{K}_6) \cdot \mathbf{r}][V_c(\mathbf{r}) + eFz] - i|J_{56}| \frac{\partial}{\partial z} \exp[-i(\mathbf{K}_5 - \mathbf{K}_6) \cdot \mathbf{r}][V_c(\mathbf{r}) + eFz] + \exp[-i(\mathbf{K}_5 - \mathbf{K}_6) \cdot \mathbf{r}][V_c(\mathbf{r}) + eFz] \left(-i|J_{56}| \frac{\partial}{\partial z} \right), \quad (15)$$

with

$$I_{56} = -\cos(2\lambda_K), \quad (16)$$

$$I'_{56} = J'_{56} = 2 \frac{\partial \lambda_K}{\partial K} \sin(2\lambda_K).$$

Here, we substituted Eqs. (12) and (13) into Eq. (7) for $l=5$ and $l'=6$ and assumed that the electric field F is in the z direction.

III. NUMERICAL RESULTS AND DISCUSSIONS

We have solved Eqs. (5)–(16) for the Si quantum-dot structure mentioned above numerically. We also considered potential quantum bit operation utilizing the intervalley interactions. In this work, we considered a quantum dot with dimensions of 8, 12, and 6 nm in the x , y , and z directions, respectively. In this structure, the ground state is associated with doubly degenerate valleys 5 and 6.

When the weak static magnetic field is applied along the growth direction, the ground-state wave function is composed of the linear combination of p -like T_1 state from the irreducible representations of T_d symmetry of the Si crystal.²⁶ In other words, the ground-state wave function is given by $|\Psi\rangle = (1/\sqrt{2})(|F_5\rangle \pm |F_6\rangle)$, where F_5 and F_6 are orbital functions for valleys 5 and 6, respectively. These orbitals satisfy the following effective Hamiltonian in the interaction picture:

$$H = \begin{bmatrix} \varepsilon(F) & \Delta(F) \\ \Delta(F) & \varepsilon(F) \end{bmatrix}. \quad (17)$$

Here ε is the energy difference between symmetric and antisymmetric states, Δ is the intervalley coupling, and F is an external electric field along the z direction. When $F=0$, both ε and Δ are zero and the total state remains unchanged because there is no intervalley coupling. In this model, we have neglected the coupling of orbitals between different axes. For example, the coupling between valleys 1 and 5 (x axis and z axis) is found to be a million times smaller than the coupling between valleys 5 and 6 (both in the z axis). If we apply an external electric field to the quantum dot, the intervalley interaction is turned on and doubly degenerate ground state is splitted. The crystal momentum necessary for the coupling of electron states between valleys 5 and 6 is provided by an applied electric field along the z direction.¹⁸

In Fig. 2, we plot the energy difference ε between the symmetric and the antisymmetric states and the intervalley coupling energy Δ which is defined as $\Delta(F) = \langle F_5 | H'_{56} | F_6 \rangle$. In

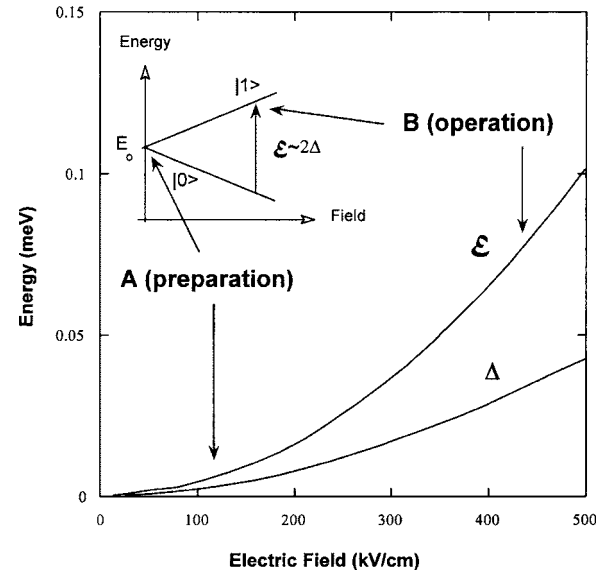


FIG. 2. We plot the energy difference ε between the symmetric and the antisymmetric states as well as the intervalley coupling energy Δ of a Si quantum dot as functions of the electric field.

this figure, one can see that the intervalley coupling is increasing rapidly with the electric field. For example, the calculated values of ε and Δ are 63.5 and 31.6 μeV , respectively, when $F=400$ kV/cm. When F is increased to 500 kV/cm, we have $\Delta=43$ μeV . These field values are below the breakdown field strength, as can be seen by the recent experimental results for the inversion layer mobility which has been measured up to 1 MV/cm.²⁷

If we turn on the electric field and wait long enough, the system would be in the symmetric state which is denoted by $|0\rangle$. The coherent evolution from the symmetric state $|0\rangle$ to the antisymmetric state $|1\rangle$ would be observed by applying the sharp voltage pulse to the pulse gate similar to the case of the Cooper-pair box¹⁰ or the double-quantum-dot structure.^{13,14} The coherent oscillation of the system is characterized by the angular frequency given by $\Omega = \sqrt{\varepsilon^2 + \Delta^2}/\hbar$, which corresponds to the microwave frequency of 17.2 GHz. When the system is evolved to the state $|1\rangle$ and if we turn off the electric field F adiabatically, the intervalley coupling would be turned off. The resulting state would be the antisymmetric orbitals which would maintain its phase coherence until the decoherence destroys the coherence.

Figure 3 shows the first six energy levels associated with valley 5 (or 6) in solid lines, valley 1 (or 2) in dashed lines, and valley 3 (or 4) in dotted line, as functions of increasing electric field. A weak magnetic field of 1.5 T is applied along the z axis. The dimension of the quantum dot used in this particular calculation is such that the ground state is associated with valley 5 or 6 in the absence of an external field. It is interesting to note that the slopes for energy levels associated with valleys 1 and 3 are similar but they are different from those of valley 5 because of the effective-mass differences along the field direction. The energy states are labeled for the single valley case, that is, when the intervalley coupling is ignored. Part of the ground-state energy level is magnified and shown in the small box inside Fig. 3. One can notice that the ground-state energy is further splitted into

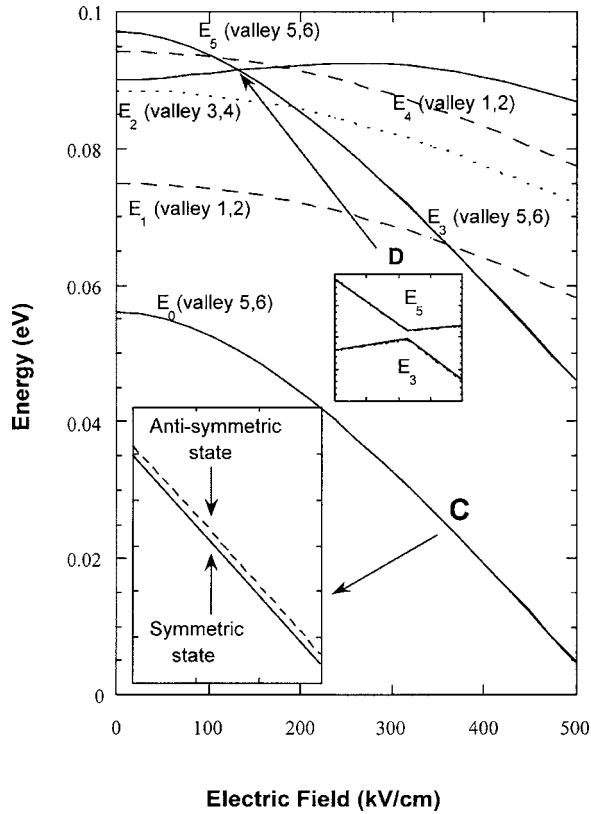


FIG. 3. We plot the first six energy levels associated with valley 5 (or 6) in solid lines, valley 1 (or 2) in dashed lines, and valley 3 (or 4) in dotted line, as functions of increasing electric field. A weak magnetic field of 1.5 T is applied along the z axis. The insets show magnified energy diagrams.

symmetric and antisymmetric states. It is interesting to see that E_3 and E_5 associated with valleys 5 and 6 show anticrossing at point D with increasing electric field. The inset shows the magnification of point D .

Details of anticrossing behavior is shown in Fig. 4 for the symmetric states (solid lines) and antisymmetric states (dashed lines) associated with E_3 and E_5 , respectively. We

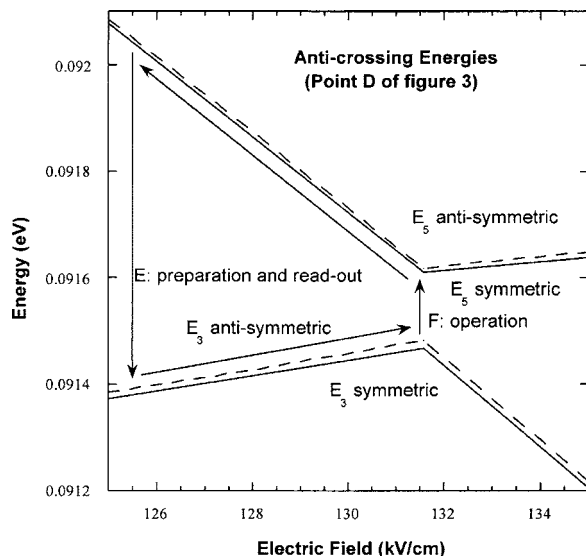


FIG. 4. Details of anticrossing behavior is shown for the symmetric states (solid lines) and antisymmetric states (dashed lines) associated with E_3 and E_5 , respectively.

found that anticrossing occurs at the field strength of 131.6 kV/cm and the energy gap is 117 μeV . At low electric field, E_3 is pushed up while E_5 is showing the negative shift with increasing electric field until anticrossing point D and their behaviors are changed the other way around after passing D . Similar behavior was observed in the case of a quantum well with an applied electric field.²⁸

The symmetric and antisymmetric splittings and other abundant features of the energy-level spectrum of Fig. 3 open up strong possibilities of realizing orbital qubits and quantum gates. The simplest example would be the controlled electric-field-induced transition between symmetric and antisymmetric states associated with valleys 5 and 6. The insets of Fig. 3 show magnified energy diagrams. We first consider the symmetric and antisymmetric states associated with E_0 (point C). Initially, we set the electric field at a low value (point A) so that transition between the two states would be difficult (Fig. 2) due to a relatively small Δ . The electron in the quantum dot is in the ground state. When the gate bias is switched to a higher electric field (point B), the time evolution between the two states would begin. The time interval of the pulse determines the relative population of the two states and they would remain at the final values when the pulse is switched back to A . The rise time of the pulse should be shorter than \hbar/Δ at A and longer than \hbar/Δ at B . On the other hand, one can also utilize the anticrossing for qubit operation shown in Fig. 4 for a qubit operation, following similar approach for the superconducting qubit.¹⁰ The qubit is prepared at E (Fig. 4) by charging an electron into the antisymmetric state associated with E_3 . We increase the electric field adiabatically to point F and then apply the microwave to start the qubit operation. The readout can be done by decreasing the electric field adiabatically to point E again. The readout of the relative population can be achieved by measuring the transport through the quantum dot. Since it is important to control both the potential and the electric field across the quantum dot, the biases of all terminals (source, drain, front gate, back gate) should be adequately adjusted.

When the ground state is associated with valleys 5 and 6 only, the wave function can be written as

$$\Psi_{S,A} = \frac{1}{\sqrt{2}} \begin{pmatrix} 1 \\ \pm 1 \end{pmatrix} \varphi_{S,A}(\mathbf{r}) = \chi_{S,A} \varphi_{S,A}(\mathbf{r}), \quad (18)$$

where $\varphi_{S,A}(\vec{r})$ are the orbital wave functions and $\chi_{S,A}$ are the pseudospins for the symmetric and antisymmetric states, respectively.

Figure 5 shows the schematic of the single qubit operation and the readout circuit. One can use a silicon-on-insulator (SOI) quantum-dot structure for qubit operation. The quantum dots are surrounded by SiO_2 and two independently tunable gates are formed on top of SiO_2 . The biases on the center gates (V_{G1} and V_{G2}) and the back gate (or the ground plane) are tuned such that the required electric field in the Si quantum dot is generated in the z direction. For $F = 300\text{--}500$ kV/cm, the quantum dot should be in the sub-threshold region. The biases on the left and right gates (V_S and V_D) induce the tunneling of an electron from dot 1 to dot 2 during the readout. The value $V_D - V_S$ is kept smaller than

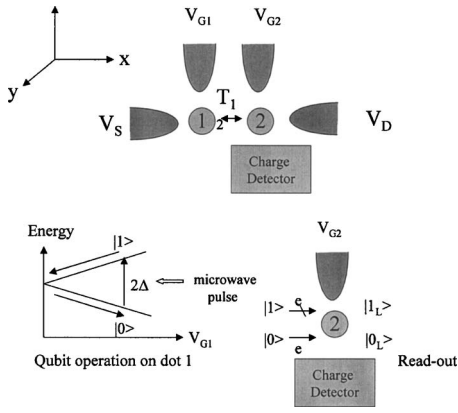


FIG. 5. Schematic of qubit operation and readout.

$k_B T$ so that the quantum dot is in the linear transport regime. In this bias scheme, F is large only in the z direction. The quantum state of the single electron injected into quantum dot 1 is the qubit and quantum dot 2, which is coupled to dot 1, acts as a readout device. The tunneling probability amplitude between dots 1 and 2 is proportional to²⁹

$$T_{12} = \int \int d\mathbf{r}_1 d\mathbf{r}_2 \varphi_a^*(\mathbf{r}_1) H_T(\mathbf{r}_1, \mathbf{r}_2) \varphi_b^2(\mathbf{r}_2) (\chi_a^1)^\dagger \chi_b^2, \quad (19)$$

where a and $b=S$ or A and H_T is the tunneling Hamiltonian. It is interesting to note that the quantum-mechanical tunneling of an electron between quantum dots 1 and 2 is parity dependent. In other words, the tunneling probability is non-negligible when the initial and final states are in the same parity states, either symmetric or antisymmetric. The σ_x operation on the qubit is achieved by the gate voltage V_{G1} and the microwave pulse. Measurement of the qubit (quantum dot 1) can be done by adjusting the gate voltage V_{G2} such that the ground state of quantum dot 2 is in resonance with the symmetric state of dot 1 while the antisymmetric states are off resonant, and by setting $V_D - V_S$ to induce the tunneling. We can also design quantum dot 2 to meet this condition. Since the energy gap 2Δ between $|1\rangle$ and $|0\rangle$ is in the order of $50 \mu\text{V}$, ambient temperature around 30 mK would be required to suppress the decoherence. From Eq. (19), one can see that the tunneling probability of the symmetric state ($|0\rangle$) would be larger than the antisymmetric state ($|1\rangle$) due to the parity selection rule. The presence or absence of an excess electron in quantum dot 2 will be denoted as the logical state $|0_L\rangle$ or $|1_L\rangle$, respectively. The excess charge of dot 2 due to the tunneling process can be measured using sensitive single-electron capacitance technique.³⁰⁻³²

We now consider the implementation of a nontrivial two-qubit gate. In Fig. 6, we show the elementary two-qubit quantum gate, which is comprised of four quantum dots, two for the two qubits and the rest for the readout. Quantum dots 1 and 2 are coupled by interdot Coulomb interaction which is also parity dependent. The interdot Coulomb interaction energy is calculated by following Beattie and Landsberg:³³

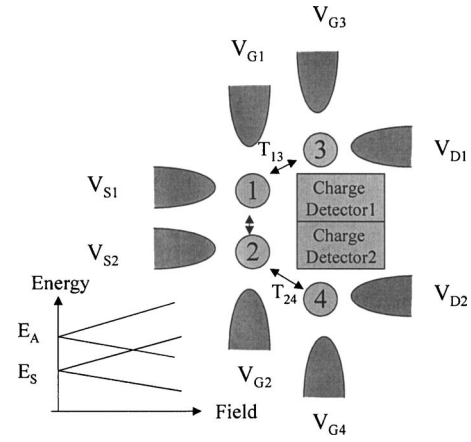


FIG. 6. Layout for the two-quantum bit gate.

$$V_{if} = \int \int d\mathbf{r}_1 d\mathbf{r}_2 [\varphi_1^*(\mathbf{r}_1) \varphi_2^*(\mathbf{r}_2) \Delta_{21} - \varphi_2^*(\mathbf{r}_1) \varphi_1^*(\mathbf{r}_2) \Delta_{12}] \times V_{sc}(\mathbf{r}_1 - \mathbf{r}_2) [\varphi_1(\mathbf{r}_1) \varphi_2(\mathbf{r}_2)], \quad (20)$$

where V_{sc} is the screened Coulomb potential; $\Delta_{21} = \Delta_{12} = 1$ when the electrons in dots 1 and 2 have the same parities; $\Delta_{21} = 1$ and $\Delta_{12} = 0$ when the electrons in dots 1 and 2 have opposite parities, which are preserved; and $\Delta_{21} = 0$ and $\Delta_{12} = 1$ when the electrons in dots 1 and 2 have opposite parities, which are both changed. The Hamiltonian for this two-electron system is given by (in $|11\rangle$, $|10\rangle$, $|01\rangle$, and $|00\rangle$ bases):

$$\hat{H} = \begin{bmatrix} E_{11} & 0 & 0 & 0 \\ 0 & E_{10} & E_C & 0 \\ 0 & E_C & E_{01} & 0 \\ 0 & 0 & 0 & E_{00} \end{bmatrix}. \quad (21)$$

Let us consider the special case of $E_{11} = 3\Delta$, $E_{10} = E_{01} = \Delta$, $E_{00} = -\Delta$, and $E_C = \delta$, and let the system evolve unitarily for the time t . The unitary evolution operator is given by

$$U = \exp(iHt) = \exp(3i\Delta t) |11\rangle\langle 11| + \left(\cos \Omega_1 t + i \frac{\Delta}{\Omega_2} \sin \Omega_2 t \right) (|10\rangle\langle 10| + |01\rangle\langle 01|) + \exp(-i\Delta t) |00\rangle\langle 00| + \left(\cos \Omega_3 t - 1 + i \frac{\delta}{\Omega_2} \sin \Omega_2 t \right) \times (|10\rangle\langle 01| + |01\rangle\langle 10|), \quad (22)$$

where $\Omega_1 = \sqrt{\Delta^2 + \delta^2}$, $\Omega_2 = \sqrt{\Delta^2 + 3\delta^2}$, and $\Omega_3 = \sqrt{2\delta\Delta}$. The last term in Eq. (22) describes the swap operation $|10\rangle \rightarrow |01\rangle$ and vice versa. If the initial state is $|10\rangle$, the resulting state after the unitary evolution for the time t will become

$$|10\rangle \rightarrow \left(\cos \Omega_1 t + i \frac{\Delta}{\Omega_2} \sin \Omega_2 t \right) |10\rangle + \left(-1 + \cos \Omega_3 t + i \frac{\delta}{\Omega_2} \sin \Omega_2 t \right) |01\rangle. \quad (23)$$

If we set $t = \pi / (2\Omega_3)$ and $\Delta = (4 + \sqrt{13})\delta$, we get

$$|10\rangle \rightarrow -|01\rangle + \cos\left(\frac{\pi\Omega_1}{2\Omega_2}\right)|10\rangle \approx -|01\rangle, \quad (24)$$

which is a swap operation followed by the phase change. In order to synthesize the controlled NOT (CNOT) operation, we need to supplement the one-qubit operation to the above operation. In passing, we would like to comment that our proposal is based on adiabatic switching of an electric field and is expected to be quite slow.

Once the valley interaction is turned off, the quantum state is supposed to evolve unitarily until the decoherence processes destroy the coherence.^{34,35} Since both F_5 and F_6 are in ground states, respectively, the only coherency destroyed by the decoherences is their relative phase. Here, we estimate the phase decoherence by the longitudinal-acoustic (LA) phonons. The upper bound of the scattering rate due to the LA phonon is given by

$$\begin{aligned} W^\pm &= \frac{2\pi}{\hbar} \sum_f \sum_q E_{ac}^2 \frac{\hbar q^2}{2V\rho\omega_q} \left(N_q + \frac{1}{2} \pm \frac{1}{2}\right) \\ &\quad \times |\langle f|e^{\mp i\mathbf{q}\cdot\mathbf{r}}|i\rangle|^2 \delta(E_f - E_i \mp \hbar\omega_q) \\ &\leq \frac{2\pi}{\hbar} \sum_f \sum_q E_{ac}^2 \frac{\hbar q^2}{2V\rho\omega_q} \left(N_q + \frac{1}{2} \pm \frac{1}{2}\right) \\ &\quad \times \delta(E_f - E_i \mp \hbar\omega_q) \\ &\approx 4\pi^2 \frac{(E_f - E_i)^3 E_{ac}^2}{\rho \hbar^4 c_l^5} \exp[-(E_f - E_i)/k_B T], \end{aligned} \quad (25)$$

where $\rho=2.33 \text{ g/cm}^3$, $c_l=9.01 \times 10^5 \text{ cm/s}$, and $E_{ac}=4.7 \text{ eV}$ for Si. For more detailed calculations of phonon scattering, we refer to the work of Fischetti and Laux.³⁶ In Fig. 7(a), we show the lower bounds of the intravalley relaxation times (or the upper bounds of the scattering rates) for different energy fluctuations as functions of the lattice temperature. In quantum dots, the phonon-scattering rates are considerably lower than those of the bulk or the quantum wells because only the transitions between discrete states are allowed. Figure 7(b) shows the estimates of decoherence time (or intravalley relaxation time) due to the LA phonons for different lattice temperatures as functions of the fluctuation energy. Both figures indicate the decoherence time of an order of 100 ns to microseconds for Si quantum-dot structures, which is considerably longer than the III-V quantum dots.

The dephasing time (or decoherence time) of the spin qubit for bulk GaAs or GaAs quantum dot is in the order of 1 ms,^{37,38} whereas the decoherence time for the charge qubit is less than 1 ns.^{9,39} The estimated decoherence time in Fig. 7 is in the same order of magnitude as that of the spin qubit and much longer than that of the charge qubit. We would also like to emphasize that our case is for the single quantum dot and with the decoherence time comparable to the spin case.

Once the external field is turned on adiabatically, the quantum state will evolve between the symmetric and anti-symmetric states and the operation time would be proportional to \hbar/Δ which is in the order of 0.1 ns. From this, we

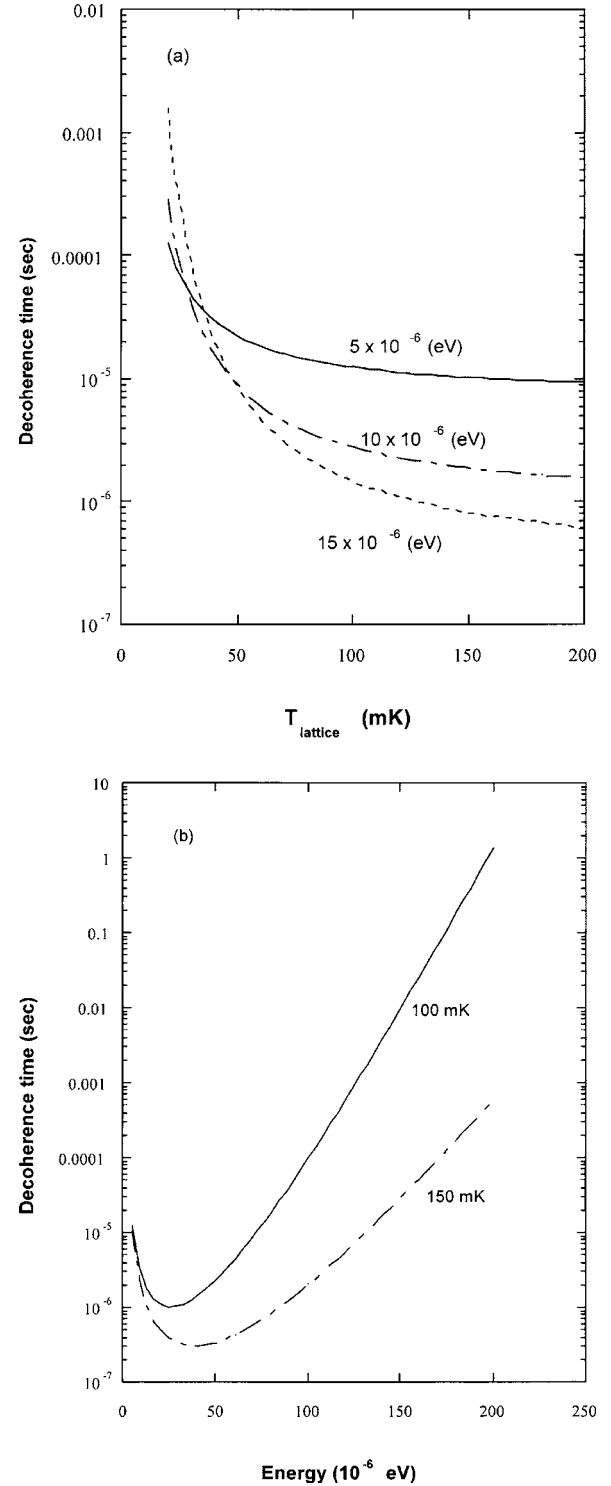


FIG. 7. (a) The lower bounds of the intravalley relaxation times (or the upper bounds of the scattering rates) for Si quantum dot for different energy fluctuations as functions of the lattice temperature due to the LA phonons are plotted. (b) We show the estimates of decoherence time (or intravalley relaxation time) for orbital qubit of a Si quantum dot due to the LA phonons for different lattice temperatures as functions of the fluctuation energy.

expect that about 1000 state evolutions (or operations) would be possible before the decoherence processes destroy the coherence of the quantum state.

IV. SUMMARY

In summary, we studied the intervalley quantum-state transitions in a Si quantum dot theoretically. We also inves-

tigated the possibility of utilizing these intervalley transitions for a quantum bit operation. Quantum bits are the multivalley symmetric and antisymmetric orbitals. Evolution of these orbitals would be controlled by an external electric field which turns on and off the intervalley interactions. Estimates of the decoherence time are made for the longitudinal-acoustic-phonon process. Elementary single- and two-qubit gates are also proposed.

ACKNOWLEDGMENTS

This work is supported by the University of Seoul through the 2004 Research Grant. The author (D.A.) also thanks D. K. Ferry, S. W. Hwang, S.-H. Park, J. H. Oh, and J. H. Lee for valuable discussions.

- ¹F. Stern and W. E. Howard, Phys. Rev. **163**, 816 (1969).
- ²A. B. Fowler, F. F. Fang, W. E. Howard, and P. J. Stiles, Phys. Rev. Lett. **16**, 901 (1966).
- ³T. Cole, A. A. Lakhani, and P. J. Stiles, Phys. Rev. Lett. **38**, 722 (1977).
- ⁴D. C. Tsui *et al.*, Phys. Rev. Lett. **40**, 1667 (1978).
- ⁵F. J. Ohkawa and Y. Uemura, J. Phys. Soc. Jpn. **43**, 907 (1977).
- ⁶L. J. Sham *et al.*, Phys. Rev. Lett. **40**, 472 (1978).
- ⁷T. Ando, A. B. Fowler, and F. Stern, Rev. Mod. Phys. **54**, 437 (1982).
- ⁸D. Loss and D. P. DiVincenzo, Phys. Rev. A **57**, 120 (1998).
- ⁹G. Burkard, D. Loss, and D. P. DiVincenzo, Phys. Rev. B **59**, 2070 (1999).
- ¹⁰Y. Nakamura, Yu. A. Pashkin, and J. S. Tsai, Nature (London) **398**, 786 (1999).
- ¹¹B. E. Kane, Nature (London) **393**, 133 (1998).
- ¹²T. D. Ladd *et al.*, Phys. Rev. Lett. **89**, 017901 (2002).
- ¹³T. Hayashi *et al.*, Phys. Rev. Lett. **91**, 226804 (2003).
- ¹⁴M. S. Jun, D. Y. Jeong, J. E. Oh, S. W. Hwang, and D. Ahn, Physica E (Amsterdam) **21**, 460 (2004).
- ¹⁵M. A. Nielsen and I. L. Chuang, *Quantum Computation and Quantum Information* (Cambridge University Press, Cambridge, 2000), and references therein.
- ¹⁶D. P. DiVincenzo, D. Bacon, J. Kempe, G. Burkard, and K. B. Whaley, Nature (London) **408**, 339 (2000).
- ¹⁷D. P. DiVincenzo, e-print quant-ph/0002077.
- ¹⁸D. K. Ferry, *Semiconductors* (Macmillan, New York, 1991).
- ¹⁹J. M. Luttinger and W. Kohn, Phys. Rev. **97**, 869 (1955).
- ²⁰W. Kohn and J. M. Luttinger, Phys. Rev. **98**, 915 (1955).
- ²¹T. H. Ning and C. T. Sah, Phys. Rev. B **4**, 3468 (1971).
- ²²S. T. Pantelides and C. T. Sah, Phys. Rev. B **10**, 621 (1974).
- ²³K. Shindo and H. Nara, J. Phys. Soc. Jpn. **40**, 1640 (1976).
- ²⁴F. J. Ohkawa, J. Phys. Soc. Jpn. **46**, 736 (1979).
- ²⁵M. Cardona and F. H. Pollak, Phys. Rev. **142**, 530 (1966).
- ²⁶F. A. Cotton, *Chemical Applications of Group Theory* (Wiley, New York, 1990).
- ²⁷S. Takagi, A. Toriumi, M. Iwase, and H. Tango, IEEE Trans. Electron Devices **41**, 2357 (1994).
- ²⁸D. Ahn and S. L. Chuang, Appl. Phys. Lett. **49**, 1450 (1986).
- ²⁹J. Bardeen, Phys. Rev. Lett. **6**, 57 (1961).
- ³⁰R. C. Ashoori, Nature (London) **379**, 413 (1996).
- ³¹T. M. Buehler *et al.*, Appl. Phys. Lett. **82**, 577 (2003).
- ³²L. C. C. Hollenberg *et al.*, Phys. Rev. B **69**, 113301 (2004).
- ³³A. R. Beattie and P. T. Landsberg, Proc. R. Soc. London, Ser. A **249**, 16 (1959).
- ³⁴D. Ahn *et al.*, Phys. Rev. A **66**, 012302 (2002).
- ³⁵D. Ahn *et al.*, Phys. Rev. A **61**, 052310 (2000).
- ³⁶M. V. Fischetti and S. Laux, Phys. Rev. B **48**, 2244 (1993).
- ³⁷J. M. Kikkawa and D. D. Awschalom, Phys. Rev. Lett. **80**, 4313 (1998).
- ³⁸T. Fujisawa *et al.*, Nature (London) **419**, 278 (2002).
- ³⁹A. G. Huibers *et al.*, Phys. Rev. Lett. **81**, 200 (1998).